nature neuroscience

Integrating motion and depth via parallel pathways

Carlos R Ponce[1,2], Stephen G Lomber[3] & Richard T Born[2]

Processing of visual information is both parallel and hierarchical, with each visual area richly interconnected with other visual areas. An example of the parallel architecture of the primate visual system is the existence of two principal pathways providing input to the middle temporal visual area (MT): namely, a direct projection from striate cortex (V1), and a set of indirect projections that also originate in V1 but then relay through V2 and V3. Here we have reversibly inactivated the indirect pathways while recording from MT neurons and measuring eye movements in alert monkeys, a procedure that has enabled us to assess whether the two different input pathways are redundant or whether they carry different kinds of information. We find that this inactivation causes a disproportionate degradation of binocular disparity tuning relative to direction tuning in MT neurons, suggesting that the indirect pathways are important in the recovery of depth in three-dimensional scenes.

Since the late 1800s it has been clear that the cerebral cortex is a modular structure[1,2]. The past several decades have seen this concept expanded, particularly in the visual system, where the work from numerous laboratories has been synthesized into a detailed hierarchical network of cortical areas[3]. Much of the current research in systems neurophysiology consists of experiments to define better how the activity of neurons in various areas relates to the perceptual, cognitive and behavioral capacities of the animal. To understand the mechanisms by which such properties arise, it is essential to determine how information represented in different cortical areas is integrated. Here we provide evidence that different visual pathways can provide modality-selective information that is integrated by single neurons to create more sophisticated representations of the visual world.

Area MT of the macaque visual cortex contains neurons that signal the direction, speed and binocular disparity of moving visual stimuli[4]. MT receives two main types of cortical input originating from layer 4B of the primary visual cortex (V1): a direct projection, and a set of indirect projections that pass through the thick stripes of area V2 and through area V3 (ref. 5 and **Fig. 1a**). Studies have suggested that the indirect pathways have a role that is complementary to that of the direct projection. First, the two pathways are anatomically segregated: most neurons in layer 4B of V1 project to one or the other, and only a few (<5%) project to both[6]. Second, the population of V1 spiny stellate cells known to project directly to MT receives strong magnocellular inputs from layer 4Cα and almost no input from the parvocellular-dominated layer 4Cβ, whereas the pyramidal neuron population that projects to V2 and V3 receives a mixed input from both sublaminae of 4C (ref. 7). Third, the direct-projecting V1 neurons are highly selective for direction[8], whereas the most prevalent response selectivity in the V2 thick stripes is for binocular disparity[9–11] rather than direction[12], and one report has shown that less than 10% of disparity-selective neurons in V2 are also selective for direction[11]. Last, although many direction-selective V1 neurons are also well tuned for disparity, neurons in V2 and MT respond to larger disparities and show odd-symmetric tuning rather than the even-symmetric tuning characteristic of most V1 neurons[13]. This observation suggests that at least some aspects of disparity tuning in MT cannot be inherited directly from V1.

In this study, we set out to define the functional contributions of the indirect pathways to the processing of visual motion and depth in MT of awake, behaving macaques. We reversibly inactivated parts of V2 and V3 in one hemisphere while recording visually evoked responses of MT neurons and smooth eye movements that are known to depend on MT activity.

RESULTS

Inactivation of V2 and V3 decreases visual responses in MT

We inactivated the indirect pathways by using small cooling loops ('cryoloops') chronically implanted in the right lunate sulcus in each of three monkeys (J, K and M; **Fig. 1b**). The three loops implanted in each monkey covered an area of roughly 8 × 18 mm (**Fig. 1c**). To confirm that activity in the lunate sulcus was silenced by cooling, we recorded visually evoked activity (by using a bar of light swept back across the receptive field) from multi-units and single units in the lower layers of the anterior bank during multiple cooling-rewarming sequences (**Fig. 1d**). Within 2–3 min of initiating cooling, visually evoked responses ceased, leaving only diminished spontaneous activity; after turning off the cooling pumps, recovery followed with a similar time course (**Fig. 1e**). Because these recording sites were located in the deepest cortical layers, at the furthest position from the cryoloops in the lunate sulcus, we are confident that all intervening layers were fully inactivated.

By contrast, MT activity was reduced only partially by cooling the indirect pathway inputs (**Fig. 2a**). At the onset of cooling, a typical MT

[1]Harvard-MIT Division of Health Sciences and Technology, Harvard Medical School, 260 Longwood Avenue, Boston, Massachusetts 02115, USA. [2]Department of Neurobiology, Harvard Medical School, 220 Longwood Avenue, Boston, Massachusetts 02115, USA. [3]Department of Physiology and Pharmacology and Department of Psychology, The University of Western Ontario, Robarts Research Institute, 100 Perth Drive, London, Ontario, Canada, N6A 5K8. Correspondence should be addressed to C.R.P. (carlos_ponce@hms.harvard.edu).

Received 9 October 2007; accepted 13 December 2007; published online 13 January 2008; doi:10.1038/nn2039

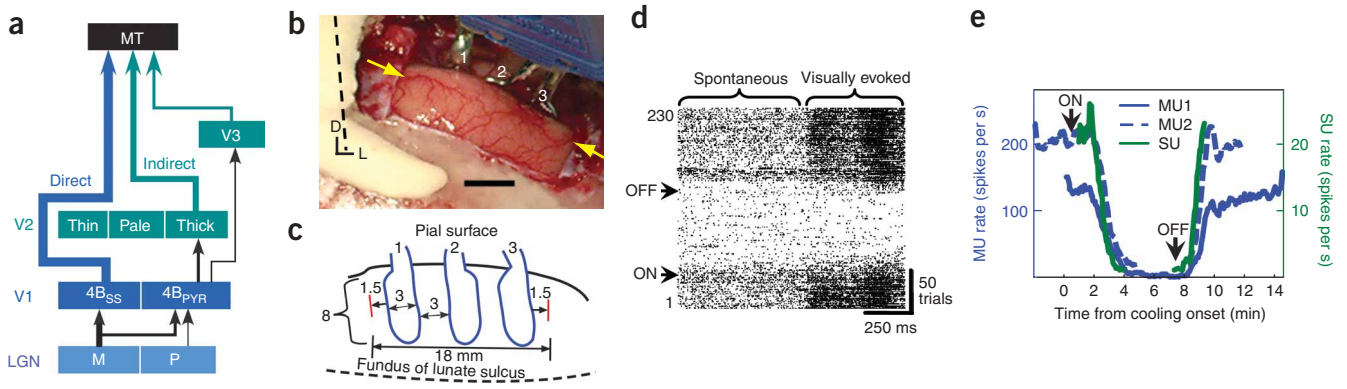

Figure 1 Effects of cooling on visually evoked activity in the anterior lunate bank. (**a**) Principal feedforward projections to MT. M, magnocellular pathways; P, parvocellular pathways; 4B, layer 4B; SS, spiny stellate cells; PYR, pyramidal cells. (**b**) Intra-operative photograph of cryoloop implants in monkey K. Image shows posterior bank of the lunate sulcus. Broken line shows the midline. Arrows point to the border between V1 and V2, which is evident from the difference in vascularity. Each cryoloop is numbered. Scale bar, 5 mm. D, dorsal; L, lateral. (**c**) Cut-away view of cryoloop placement along the posterior bank of the lunate sulcus. The surface of the brain is at the top; the fundus of the lunate sulcus is represented by the broken line at the bottom. Cryoloops were implanted in the lunate sulcus of the right hemisphere in three different monkeys and lowered to a temperature of 0–6 °C to inactivate all cortical layers. All distances are in millimeters. (**d**) Raster plot showing spontaneous and visually evoked multi-unit responses from layers 5/6 in the anterior lunate bank. Each row shows a single trial of the neural response to a light bar at the preferred orientation moving into the receptive field. Arrows indicate the time points when cooling pumps were turned on and off. (**e**) Mean multi- (MU) and single-unit (SU) responses from neurons in layers 5/6 of the anterior bank of the lunate sulcus. Curves show the firing frequency aligned at the onset and termination of the cooling pump cycle. Each point is the running average of three stimulus sweeps.

neuron gradually became less visually responsive and, within 5 min, stabilized at a lower firing rate. When cooling was discontinued, the firing rate returned to almost the pre-cooling level with a similar time course (**Supplementary Fig. 1** online). For each neuron in our sample, the steady-state change in response was quantified with a 'blocking index'[14] (see Methods), revealing a modest reduction in firing rate for most MT neurons during cooling of V2 and V3 (hereafter V2/V3; **Fig. 2b**, 42 single units and 38 multi-unit clusters from monkeys K and M; median blocking index = 0.20). As a measure of the retinotopic extent of the V2/V3 inactivation, we plotted this distribution of blocking index as a function of receptive field location (**Fig. 2c**). The effects were strongest for neurons with receptive fields in the lower contralateral hemifield, as expected from the known visual representations of V2 and V3 in the lunate sulcus[15,16].

Direction tuning in MT is well preserved without V2/V3

Despite these changes in firing rate, direction-tuning properties in MT remained relatively unaltered in the absence of input from V2/V3. **Figure 3a** shows a set of direction-tuning curves obtained from a single unit before, during and after inactivation of the indirect pathways. Each curve can be summarized by its mean vector, whose direction corresponds to the preferred direction of the neuron and whose length indicates tuning width. During cooling, there was a decrease in firing rate but the preferred direction and tuning width did not change significantly, a finding typical of most neurons in our sample (**Fig. 3b**). Eighty-four percent of neurons did not show a significant change in their preferred direction during inactivation ($P < 0.05$, Watson-Williams test; $n = 74$ neurons significantly tuned to direction before cooling, $P < 0.05$, one-way analysis of variance (ANOVA)), and the median absolute change in preferred direction for the 12 neurons that did show a significant change was only 6°. Tuning width was more variable (**Fig. 3c**): most pre-cooling and cooling tuning widths were not significantly different (70%, $P > 0.05$, Wilcoxon rank sum test), and a few became either narrower (18%) or wider (12%). From these data, we conclude that input from V2/V3 is not essential for the direction tuning of MT neurons, and, in some cases, may partially degrade this selectivity.

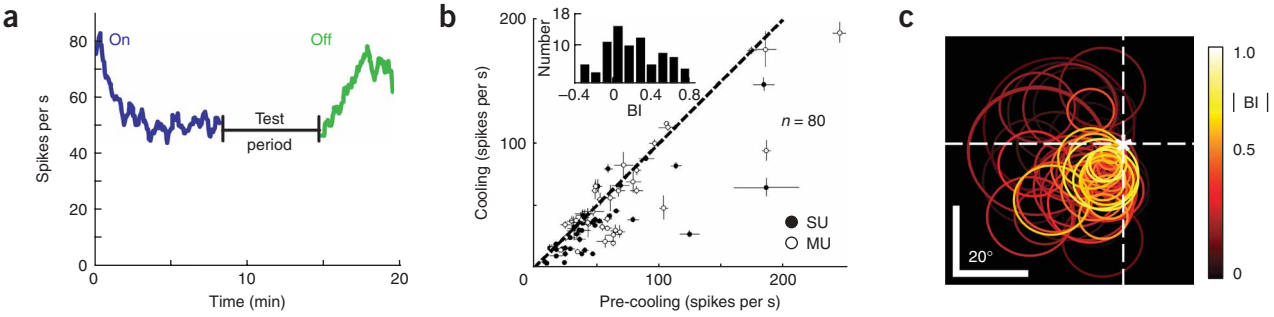

Figure 2 Effects of V2/V3 inactivation on the firing rates of MT neurons. (**a**) Responses of an individual MT neuron to its preferred stimulus at cooling onset (blue curve) and during rewarming (green line). (**b**) Population change in mean firing rate. Each point shows the response of a single recording site before and during cooling (mean ± s.e.m., $n = 80$). Inset, distribution of the blocking index, BI (median blocking index = 0.20). (**c**) Distribution of blocking index as a function of receptive field position in visual space. Each circle represents the location and approximate size of a hand-mapped response field; its color represents the absolute value of its corresponding blocking index.

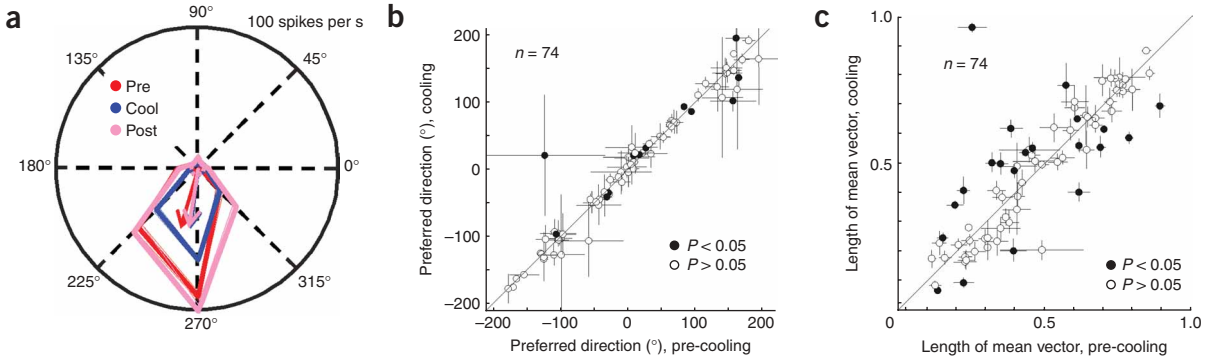

Figure 3 Changes in direction tuning of MT neurons during V2/V3 inactivation. (**a**) Direction-tuning curves measured for a single unit in MT before (red), during (blue) and after (magenta) cooling of the indirect pathways. Mean ± s.e.m. responses are presented in polar coordinates; arrows indicate the mean vector of each tuning curve (vector lengths have been multiplied by maximum firing rate). (**b**) Preferred directions recorded before and during cooling (error bars indicate 95% CI, $n = 74$). Filled points represent neurons that showed statistically significant changes in preferred direction ($P < 0.05$, two-sample Watson-Williams test). (**c**) Changes in tuning bandwidth during cooling (mean ± s.e.m.). Points below and above the equality line represent neurons that became, respectively, more broadly and more narrowly tuned. Filled symbols indicate statistically significant changes in mean vector length ($P < 0.05$, Wilcoxon rank sum test, $n = 74$).

V2/V3 inputs are more important for disparity tuning in MT

This finding contrasts with tuning for binocular disparity, which was markedly impaired in the same neurons. **Figure 4a** shows direction- and disparity-tuning data from three MT units recorded before and during V2/V3 inactivation. During cooling, these units showed a decrease in firing rate that produced scaled-down direction-tuning curves without significant degradation (or, as in the rightmost unit, with an observable improvement) of their mean directional properties. Their binocular disparity–tuning curves, however, were more adversely affected by cooling, showing decreased modulation that often resulted in flatter curves.

As an initial measure, we used a discrimination index[17] (DI; see Methods) to compare the relative effects of the inactivation between both visual modalities. The first and second units showed small decreases in direction discriminability during cooling ($\Delta DI = DI_{pre\text{-}cooling} - DI_{cooling}$; $\Delta DI = 0.04$ and 0.02, respectively) but correspondingly larger degradations in disparity ($\Delta DI = 0.37$ and 0.11). The rightmost unit showed a smaller decrease in disparity discriminability ($\Delta DI = 0.03$), but an increase in direction discriminability ($\Delta DI = -0.18$). We selected the subset of neurons that, before cooling, were significantly tuned to both direction and disparity ($P < 0.05$, one-way ANOVA, $n = 41$) and compared their DIs (**Fig. 4b**). As previously shown[18], baseline MT responses were more strongly modulated by stimulus direction than by binocular disparity. During cooling, direction DIs showed relatively less change than did disparity DIs: the median index changes (control minus cooling) for direction and disparity were 0.04 and 0.14, respectively, both of which were significantly larger than zero ($P < 0.001$, Wilcoxon signed rank test for zero median). The median change in disparity DI was significantly larger than that in direction DI ($P < 0.01$, one-tailed Mann-Whitney test).

Discrimination indices, although useful as a means of comparison, reflect only the extent of neural modulation defined by the maximum and minimum responses. Visual inspection of the binocular disparity–tuning curves obtained during cooling (**Fig. 4a**) indicated that many of the neurons seemed either to lose tuning or, in some cases, to change their shape. We thus performed two additional analyses that took into account the neural responses to all visual stimuli. The first was to perform a one-way ANOVA and to test whether there was a significant ($P < 0.05$) main effect of stimulus condition (recall that we applied this test to the pre-cooling tuning curves to limit our analyses to neurons that were initially sensitive to both stimulus direction and binocular disparity). Of the MT neurons that were originally tuned for both, over a third (36%) failed the ANOVA test for binocular disparity tuning during cooling, but only 8% lost tuning for direction by the $P < 0.05$ criterion. As we made the ANOVA criterion for both pre-cooling and cooling tuning curves more stringent (decreasing P from 0.05 to 0.01 to 0.001), the proportion of neurons losing direction selectivity remained almost unchanged (in fact it decreased slightly to 7% and then 5%),

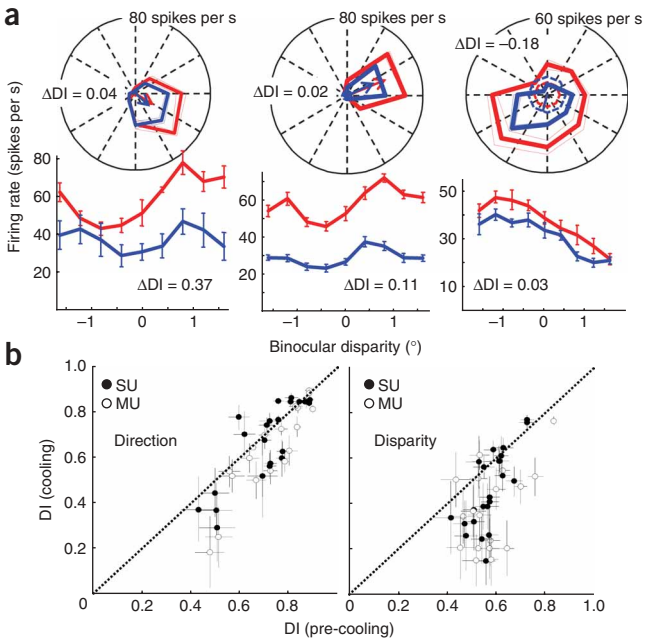

Figure 4 Comparison of changes in disparity and direction tuning of MT neurons during V2/V3 inactivation. (**a**) Paired sets of direction and disparity (mean ± s.e.m.) tuning curves recorded from the same sites before (red) and during (blue) cooling. ΔDI values show the changes in DI for direction and disparity ($\Delta DI = DI_{pre\text{-}cool} - DI_{cool}$). (**b**) DI values before and during cooling for direction (left) or disparity (right). Open symbols, multi-unit sites; filled symbols, single-unit recordings (mean ± s.e.m., $n = 41$). Broken diagonal lines indicate the line of equality.

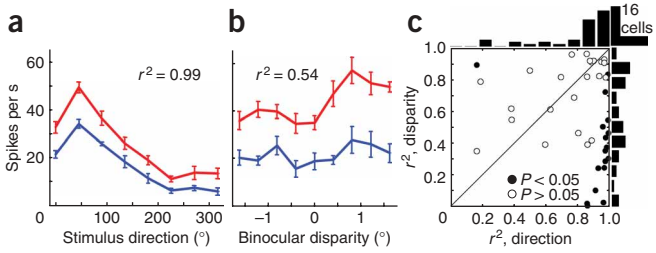

Figure 5 Quantitative and qualitative changes in tuning for direction and disparity during V2/V3 inactivation. (**a**,**b**) Direction- and disparity-tuning curves (mean ± s.e.m.) recorded from the same neuron before (red) and during (blue) cooling. The correlation coefficients (r^2) of determination for direction and disparity were 0.99 and 0.54, respectively. (**c**) Correlation between pre-cooling and cooling tuning curves for direction and disparity. Each circle represents a recording site. Abscissa shows the r^2 value for direction; ordinate shows the r^2 value for disparity. Filled symbols indicate that both r^2 values are significantly different from each other ($P < 0.05$, ref. 19).

whereas that for binocular disparity increased to 39% ($P < 0.01$) and then 47% ($P < 0.001$). Thus, we found a marked difference in the proportions of MT neurons that completely lost tuning to the different visual modalities (binocular disparity versus direction) during inactivation of the indirect pathways, and this difference was robust to changes in the criterion to assess tuning.

As a further test for changes in the shape of tuning curves, we computed the linear correlation coefficient (r) between each neuron's control (pre-cooling) and cooling tuning curve for each modality. If a tuning curve is simply a scaled version of its pre-cooling counterpart, modified through a change in either tuning-curve amplitude (gain) or baseline activity (offset), then the correlation coefficient will be equal to one. We then tested whether the direction and disparity correlation coefficients measured from the same cell were statistically different from each other. For the single-cell example shown in **Figure 5a**,**b**, the direction-tuning curves (**Fig. 5a**) were highly correlated across experimental conditions ($r^2 = 0.99$, $P < 0.0001$, Student's t-test). In comparison, the disparity-tuning curves of this neuron (**Fig. 5b**) were less well correlated ($r^2 = 0.54$, $P = 0.023$) and the disparity correlation coefficient was significantly smaller than the corresponding direction value ($P < 0.001$, ref. 19). Across the population of MT neurons, 68% (28 of 41) of all direction-tuning correlation coefficients were larger than the corresponding disparity values, and 61% of these coefficients were statistically significant (17 of 28 cells, $P < 0.05$, ref. 19; **Fig. 5c**). Only one disparity correlation coefficient was significantly larger than its directional counterpart.

A trivial cause for the selective loss of disparity tuning would be that inactivation of V2/V3 impairs the ability of the monkeys to stabilize their gaze in depth (vergence) during fixation. However, we continuously monitored the position of both eyes during all experiments and found no systematic changes in the vergence state of the monkeys during inactivation of V2/V3 (**Supplementary Fig. 2** online). Thus, our results are not due to impaired gaze control during fixation. Rather, they suggest that the indirect pathways enhance the modulatory effects of binocular disparity on MT neurons and have a less important role in encoding the direction of motion.

Differential effects are not due to a global gain change

Two alternative physiological mechanisms might account for this effect revealed by cooling. The indirect pathways might arise from a subset of neurons in V2 and V3 that are more strongly tuned for binocular disparity and less tuned for the direction of motion. Alternatively, it is possible that the overall stimulus selectivity of neurons in the two pathways is similar but, because MT neurons are less sensitive to binocular disparity (as compared with direction), a nonselective decrease in visually evoked responses might affect disparity tuning more severely. We refer to the latter possibility as the 'global gain hypothesis'. **Figure 4b** illustrates these two alternatives. These plots show that the disparity DI data fall mostly below the identity line, whereas the direction DI data are closer to it. However, the disparity DI distribution has lower pre-cooling values as compared with the direction DI distribution; thus, it is possible that all of the direction and disparity data fall along a single regression line, which would favor the global gain hypothesis.

To address this issue, we fitted regression lines to each distribution (pre-cooling versus cooling) for direction and disparity by using a Model-2 maximum likelihood fit, which minimizes the error in both x and y while weighting the contribution of each point by its standard error (**Supplementary Fig. 3** online). Both fits were highly significant ($P < 0.0001$), but the parameters describing the regression lines for disparity (slope = 1.72 ± 0.08, y intercept = −0.55 ± 0.06, $n = 41$) and direction (slope = 1.27 ± 0.06, y intercept = − 0.23 ± 0.05, $n = 41$) were clearly different ($P < 0.01$). These fits were performed on all of the data, that is, both single- and multi-unit sites. Because cooling effects at multi-unit sites are more difficult to interpret, we repeated the fits using only sites at which single-unit isolation was confirmed for all tests (see Methods). For these data ($n = 23$), the differences were even more profound: the relationship for disparity became steeper (slope = 2.15 ± 0.15, y intercept = −0.77 ± 0.10), whereas that for direction became statistically indistinguishable from the line of equality (slope = 1.06 ± 0.08; y intercept = −0.05 ± 0.06), indicative of no effect. Lastly, the data were significantly better described by two separate regression lines (one for direction and one for binocular disparity) than by a single regression line ($P = 0.0027$, sequential F-test). Thus, we can reject the possibility that all of the data lie along a single line.

We performed two further analyses to test and ultimately to rule out the global gain hypothesis. First, we tested whether the relative gain changes for direction and binocular disparity were correlated for

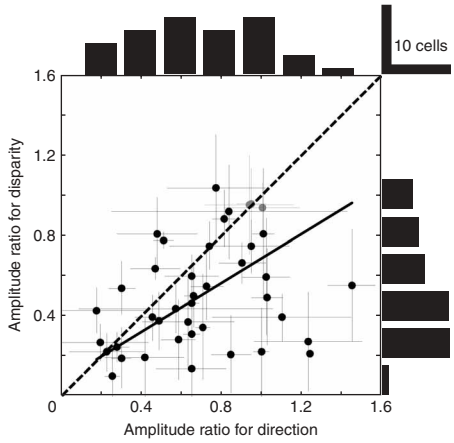

Figure 6 Correlation of direction and disparity modulation-amplitude ratio distributions. Each point represents a recording site. Abscissa shows the modulation amplitude ratios (mean ± s.e.m.) computed for direction, ordinate shows the ratios for disparity (where modulation amplitude ratio = $(R_{max} - R_{min})_{cool}/(R_{max} - R_{min})_{pre\text{-}cool}$). Standard error bars were derived through bootstrapping (500 iterations). Gray circles indicate units that showed no significant change in amplitude ratio for either visual modality.

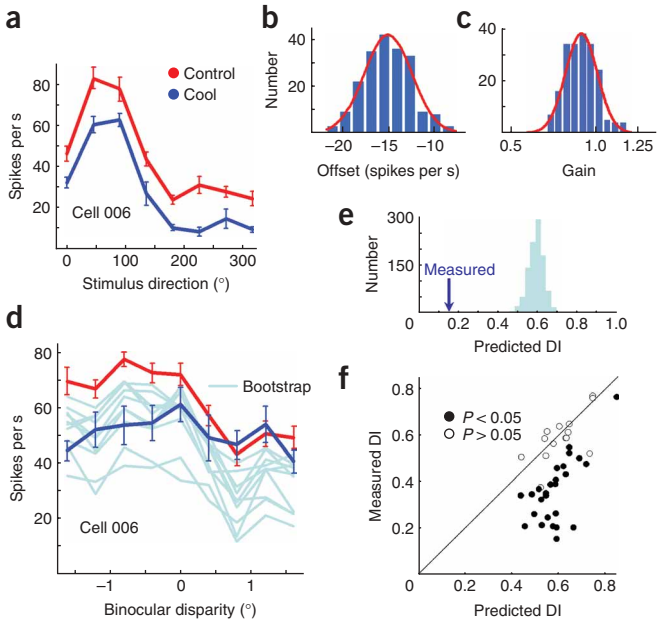

Figure 7 Bootstrap test of the global gain hypothesis. (**a**) Direction-tuning curves recorded before (red) and during (blue) cooling (mean ± s.e.m.). (**b**,**c**) Gain and offset distributions obtained by bootstrapping direction-tuning data (200 iterations). (**d**) Disparity-tuning curves recorded before (red) and during (blue) cooling (mean ± s.e.m.). Light blue traces are example bootstrap disparity-tuning curves calculated by resampling pre-cooling disparity data and applying direction gain and offset values sampled randomly from the distributions in **b** and **c**. (**e**) Predicted disparity DI distribution from bootstrap (1,000 iterations). Blue arrow indicates the actual DI value obtained during cooling. (**f**) Plot of predicted disparity DI against measured cooling disparity DI values. Each point represents a recorded site. Abscissa shows the mean predicted disparity DI values; ordinate shows the measured values ($n = 41$).

individual neurons. Under the global gain hypothesis, the correlation should be nearly perfect. The modulation-amplitude ratios ($[R_{max} - R_{min}]_{cool}/[R_{max} - R_{min}]_{pre\text{-}cool}$) for each neuron, however, were only weakly correlated across the MT population ($r^2 = 0.10$, $P = 0.043$, Fisher's test; **Fig. 6**). Even this small degree of correlation may be misleading, however, because it can be artificially inflated by including sites where neither modality is affected, such as neurons with receptive fields outside the region of the visual field affected by the cryoloops. We therefore repeated this analysis for the subset of neurons in which at least one of the modalities was significantly affected ($0.9 \geq$ amplitude-modulation ratio ≥ 1.1, three data points excluded; **Fig. 6**, gray) and found that the correlation between modalities disappeared ($r^2 = 0.06$, $P = 0.15$, Fisher's test). Thus, neurons that present the best test of the global gain hypothesis provide no evidence in support of this hypothesis.

A second and more specific test of the global gain hypothesis would be to reproduce the observed cooling responses to one modality given the functional change produced by the other. In particular, we wanted to test whether the gain and offset changes that we observed for direction-tuning curves could produce the changes in discrimination that we observed for binocular disparity, which would support the global gain hypothesis. To examine this, we used sequential bootstrap procedures on each neuron (**Fig. 7**). First, we used a bootstrap procedure to obtain estimates of the variability in gain and offset observed in the direction-tuning data: raw spike counts were resampled to generate 200 new sets of pre-cooling and cooling tuning curves, which were then used to obtain distributions of both gains (defined as the modulation-amplitude ratios; **Fig. 7b**) and offsets (where offset was defined as $R_{min\text{-}cool} - R_{min\text{-}pre\text{-}cool}$, **Fig. 7c**). In a subsequent bootstrap (**Fig. 7d**), we resampled the pre-cooling disparity-tuning data and, for each individual spike count sample drawn from the disparity data, we drew gain and offset values randomly from the previously obtained direction-based distributions, applying these changes to each new disparity sample. From these repeated samples, we derived a new population of disparity-tuning curves ($n = 1{,}000$; **Fig. 7d**, light blue lines) and used these curves to generate predicted disparity DIs under the global gain hypothesis (**Fig. 7e**). This distribution of predicted DI was then compared with the experimentally determined DI (**Fig. 7f**).

The measured DI of most neurons (63%) fell outside the 95% confidence interval (CI) predicted by the global gain hypothesis, and all of these values were smaller than the DI predicted from the direction-tuning data. Thus, most MT cells showed a disproportionate degradation of their binocular disparity tuning that could not be accounted for by the changes in gain and offset measured from their corresponding direction-tuning curves.

Disparity-dependent vergence is impaired without V2/V3

Many areas in the visual hierarchy contain high percentages of disparity-tuned cells[20], and it seemed possible that these additional regions might compensate for the temporary loss of depth information caused by V2/V3 inactivation. In addition to its role in the perception of motion and depth[21], MT and its primary target region, the medial superior temporal (MST) area, have been strongly associated with the initiation of smooth eye movements that stabilize gaze, such as smooth pursuit[22,23], ocular following[24] and vergence[25–27]. We tested whether the effects that we observed on MT neurons had a behavioral correlate by examining the effects of cooling V2/V3 on binocular disparity–dependent eye movements, such as vergence. The disparity stimuli were random dot textures, 20° in diameter, and centered in the lower left quadrant of the visual field, contralateral to the inactivated sulcus. The monkeys were required to begin each trial by fixating on a 0.7° circle located 10° right of the center of the monitor. After 2–3 s of fixation, this target was extinguished and a new fixation target appeared at the center of the monitor, at which point the monkey was required to make a centering saccade to the new target. After 10–20 ms, a disparity step was introduced in the static random dot texture. Vergence velocity was measured over a window of 40–50 ms (see Methods) and plotted against stimulus disparity to construct vergence-tuning curves.

Vergence responses continued to minimize the induced disparity error across all temperature conditions: vergence angle increased toward small crossed disparities, and decreased in response to

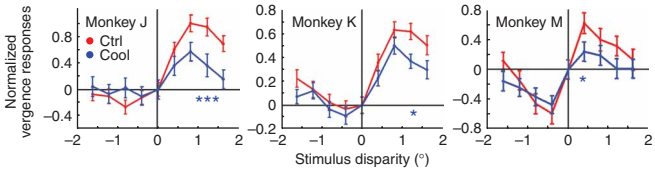

Figure 8 Effects of V2/V3 inactivation on disparity-dependent eye movements. Shown are vergence-tuning curves as a function of temperature condition. Normalized vergence velocity responses (mean ± s.e.m.) were plotted against stimulus binocular disparity before (red) and during (blue) cooling for monkeys J, K and M. Asterisks indicate responses that were significantly different, as determined by a multiple comparison procedure (see text).

uncrossed disparities (**Fig. 8**). Inactivation of V2/V3 caused a significant reduction in the gain of vergence responses in all monkeys ($P < 0.001$, one-way ANOVA, temperature condition), especially when elicited by larger disparity steps ($P < 0.05$, two-way ANOVA, temperature condition versus stimulus disparity, using the multcompare.m function in Matlab). These results show that, during V2/V3 inactivation, the oculomotor system did not compensate for externally imposed binocular disparity errors as efficiently as in the pre-cooling condition. These findings are consistent with the loss of disparity discriminability observed in our neurophysiological data. In addition, another study has shown a similar but more severe deficit after chemical inactivation of motion-processing areas in the superior temporal sulcus[27], which supports the idea that this behavioral effect involves the V2/V3 to MT pathway.

DISCUSSION

We have shown that reversibly inactivating retinotopic regions of V2 and V3 disrupts the selectivity of MT neurons for binocular disparity to a significantly larger degree than their selectivity for direction of motion. For several reasons, we think it is highly probable that the effects that we have observed result from inactivation of the feedforward indirect pathways (V1→V2/V3→MT) and not from altered feedback to V1 influencing the direct pathway (V2/V3→V1→MT).

First, the effect of V2 inactivation on V1 neural responses seems to be weak and highly variable[28,29]. In the sole study in which macaque V2 was inactivated while V1 activity was monitored[28], only about 10% of V1 neurons were found to be significantly affected and these neurons showed an average decrease in activity of roughly 40%. Second, feedback projections seem to be much less selective, as compared with feedforward projections, and thus less likely to produce the sort of modality-selective effects that we have observed. For example, one study that analyzed the visual response properties of V1 neurons that either projected to (feedforward) or received projections from (feedback) MT found that the former are very homogeneous and highly specific, whereas the latter are extremely heterogeneous and seem to span the whole range of response properties found in V1 (ref. 8). These findings, combined with the effects that we observed on large binocular disparities (which are not represented in V1; ref. 30), argue that our effects resulted from disruption of the feedforward projections of the indirect pathway.

Our results raise several issues. It is known that some complex cells in V1 provide an integrated calculation of motion and depth—so-called 'joint encoding'[31–33]; thus, one might ask why MT uses separate input pathways. One answer may be that the information needs to be combined in specific ways, and calculating each modality separately is necessary to achieve this. Indeed, studies have shown that there is marked specificity in the interactions between direction and binocular disparity: for example, most MT cells are inhibited by null direction motion most effectively when the stimulus is presented at the preferred binocular disparity[34]. Such disparity-selective motion opponency would tend to force conflicting motion cues to occupy different depth planes, thereby providing a potential neural mechanism for surface segmentation based on motion and depth[35,36].

Another advantage to parallel computation is that each modality can be more robustly encoded by pooling across specific dimensions that might impair representation of the other dimensions—an example of computational 'complementarity'[37]. For example, reliable measurements of motion direction require a comparison of local motion signals arising from edges at different orientations, whereas the determination of horizontal disparity requires precise binocular matches of vertically oriented edges. Combining information from several orientations improves the former, but would degrade the latter. Some computational models of motion processing have solved this problem by introducing separate stages for depth and direction analysis[38].

It is also clear that MT neurons represent considerably larger disparities than do V1 cells[13], in contrast to the spatial range of motion computations, which are nearly equivalent in V1 and MT[39,40]. Part of the reason for this difference may be that motion is usually continuous (except during periods of occlusion), and thus even small V1 receptive fields can encode a reasonable range of speeds. Depth, by contrast, is often discrete, and natural scenes produce relatively large horizontal disparities that could easily 'jump' the disparity limits of small V1 receptive fields. Neurons in V2 and V3, with their larger receptive fields[41,42], might provide the necessary extension in the spatial range of disparity encoding.

Lastly, the need to combine information from the two modalities in an orderly way may create developmental problems that necessitate parallel pathways. MT contains orderly representations of both direction of motion[43] and binocular disparity[44]; in addition, these two maps are related to each other in a nonrandom way[44]. Although the exact function of this relationship remains unknown, its very existence and reproducibility in different animals argue that it is significant. It may be that creating such an orderly alignment of two different maps requires organization of one or the other before the stage at which they are combined. From this perspective, the report of a disparity map in the thick stripes of V2 (ref. 45), which provide the bulk of the indirect inputs to MT, is particularly interesting. Techniques that facilitate more detailed analysis of the functional organization of the V2 outputs, such as two-photon imaging of Ca^{2+} signals[46], and those that permit more precise circuit manipulation, for example, virally encoded light-gated ion channels[47], promise new directions of research that can probe these issues in greater depth.

METHODS

Behavioral tasks. Three male macaques (*Macaca mulatta*, 7–10 kg) were seated comfortably in custom chairs (Crist Instruments). The monkeys were trained to fixate a zero-disparity 0.7°-diameter ellipse (within a 2–3° window) for 2–3 s to receive a juice reward. During binocular disparity–tuning experiments, the fixation ellipse was surrounded by a small 3°-wide patch of zero disparity dots to help to anchor vergence. In the vergence experiments, the monkeys began a trial by fixating on an eccentrically placed spot (10° right of center) for 2–3 s while we displayed a stationary random dot pattern (RDP; diameter = 20°) at zero disparity centered off the fovea, at (−7.5, −7.5)° relative to the center of the monitor. Monkeys were then required to make a saccade to a center fixation point. As the monkey's gaze arrived at the center window, we introduced a disparity step to the RDP for 150 ms (disparity values ranged from −1.6° to 1.6° in steps of 0.4°). A brief juice reward was granted if the monkey maintained gaze within the central 20° for the whole duration of the stimulus. All procedures were approved by the Harvard Medical Area Standing Committee on Animals.

Visual stimuli. For lunate sulcus recordings, stimuli were simple light bars swept across the receptive field (~1.5° wide) at the preferred orientation of the site. For MT experiments, stimuli consisted of circular patches of random dots (1 dot per degree^2; each dot was 0.3° wide) displayed in a ViewSonic P225f monitor at a refresh rate of 100 Hz. The monitor distance was 39 cm, covering ~55° of the horizontal visual field. Random dot patterns in disparity-tuning experiments consisted of dot pairs, one red and the other cyan, which were offset horizontally by a variable distance. The monkeys viewed this stimulus through monocular filters colored red or cyan (Kodak gelatin filters, nos. 29 and 44a), so that only one set of dots was visible to each eye. Red/green/blue monitor gun values were set at photometric equivalence (~11 cd/m^2), as measured through the color filters, and had a crossover of 3–6%.

Experimental protocol and cooling procedure. Area MT was located by using structural magnetic resonance imaging scans aligned to the recording grid, the well-established relationship between receptive field width and eccentricity, and the high frequency of direction-tuned neurons. After isolating a single unit or multi-unit cluster, we mapped receptive field position and size by using a small moving or flashing bar. The analog voltage signals from the extracellular recordings were digitized at 25 kHz and saved to computer disk by using a Cambridge Electronic Design 1401 data acquisition system. Spike2 software was used to confirm single-unit isolation or track changes in the signal composition of multi-unit recordings. Direction-tuning data were obtained by using RDPs moving in eight directions (0° to 315° in 45° steps) at the preferred speed and 0° disparity; disparity-tuning data were obtained with stimuli moving in the preferred direction or speed at binocular disparities ranging from −1.6° to +1.6° in steps of 0.4°. Cell clusters were not always tested for all tuning responses. Each stimulus presentation had a motion-onset delay of 240 ms after appearance and was presented an average of seven times.

After collecting a set of pre-cooling tuning data, we started the cooling process by running chilled methanol through the cryoloops until they reached temperatures between 0 and 6 °C, which usually brings cortical temperature down to 20 °C within a range of 1.6 mm (ref. 48). We collected the responses of each unit to its preferred and null directions (at the optimal speed and zero disparity) immediately after turning on the pumps to track the time dependency of the cooling process (stabilization usually occurred at 5–7 min after cooling was started). We then obtained a new set of tuning curves, tracked the firing rate during rewarming, and measured post-cooling tuning curves if the units remained properly isolated. The complete data cycle usually lasted between 40 and 60 min.

Data analysis. Tuning curves for our neurophysiology data were calculated from data collected in the first 500 ms after motion onset. The blocking index was calculated as $1 - (R_{cool}/R_{pre\text{-}cool})$, where R_{cool} and $R_{pre\text{-}cool}$ are the responses in spikes per second to the preferred stimulus. ANOVA tests for significance of tuning were performed by using the square root of the firing rates to homogenize the variance across different stimulus responses. For the direction-tuning analysis, we selected the subset of cells that were tuned to direction ($P < 0.05$, one-way ANOVA) and had a directional index above 0.5 (defined as $\mathrm{DirI} = 1 - \frac{R_{min}}{R_{max}}$, where R_{max} is the maximum mean response and R_{min} is the response in the null direction). For each neuron, we calculated a set of N pre-cooling and cooling mean directional vectors (where N is the number of completed trial sets, usually seven trials per stimulus direction) and tested for significant differences between the pre-cooling and cooling sets by using a Watson-Williams test (for the vector angle) and Wilcoxon rank sum test (for the vector length). We also tested for differences at the population level ($P > 0.05$ for both Watson-Williams and paired t-tests; mean pre-cooling versus mean cooling directional vectors). For the analysis of direction- versus disparity-tuning effects, we restricted our comparison to the subset of neurons that were significantly tuned for both direction and disparity ($P < 0.05$, one-way ANOVA). Discrimination indices[18,30] were calculated as

$$\mathrm{DI} = \frac{(R_{max} - R_{min})}{(R_{max} - R_{min}) + 2\sqrt{\mathrm{SSE}/(N - M)}}$$

where R_{max} and R_{min} are the responses to the preferred and null direction or disparity, SSE is the squared sum error around the mean response to each trial type, N is the number of trials, and M is the number of stimulus types (eight for direction, nine for disparity). Pre-cooling and cooling discrimination indices were computed using responses to the same stimulus parameters.

To determine the disparity-dependent vergence-tuning curves, dual eye position and velocity (analog differentiator: low-pass, −3 dB at 50 Hz) were digitized and stored to disk at 250 Hz for off-line analysis. Vergence was calculated by subtracting the position and velocity signals of the right eye from those of the left. Because rightward positions are conventionally positive, crossed (near) disparities are also positive and upward deflections indicate increased convergence. Trials were rejected if saccades occurred in the first 140 ms after stimulus onset. Analysis windows for vergence-tuning curves were determined by identifying the periods after disparity onset when vergence responses first become significantly different from each other ($P < 0.05$, one-way ANOVA tests performed at each 4-ms time bin). The earliest disparity-specific responses for monkeys J, K and M started at 116 ms, 100 ms and 76 ms, respectively. Although this method overestimates the actual response latency, our reported eye movement data do show longer latencies and smaller magnitude responses than those presented previously[26,49,50]; however, previous studies used large (>40°) visual textures that were centered at the fovea. The stimuli in our experiments were located off the fovea and restricted in size (20° wide) to the lower quadrant, where we expected the largest cooling effects. Eye velocity was averaged over the above time window and plotted against stimulus disparity after subtracting the response to the zero-disparity condition to eliminate post-saccadic vergence drift. This approach forced all disparity-tuning curves to pass through the center of the plot.

Note: Supplementary information is available on the Nature Neuroscience website.

ACKNOWLEDGMENTS

We thank P. Hendrickson and A. Zaharia for technical assistance, and J.H.R. Maunsell, J.A. Assad, M. Livingstone and N. Price for comments on the manuscript. This work was supported by a grant to C.R.P. from the National Institutes of Neurological Disorders and Stroke (F31NS052926), a grant to S.G.L. from the Natural Sciences and Engineering Research Council of Canada (327442), an R01 grant to R.T.B. (EY11379), a Vision Core Grant (EY12196) and a gift from R. Brandon Fradd.

AUTHOR CONTRIBUTIONS

R.T.B. conceived the initial inactivation project. C.R.P. performed the experiments and developed the project along with R.T.B. S.G.L. fabricated the cryoloops and, along with R.T.B., implanted them in all monkeys. C.R.P. and R.T.B. wrote the manuscript, and all authors participated in its editing.

Published online at http://www.nature.com/natureneuroscience
Reprints and permissions information is available online at http://npg.nature.com/reprintsandpermissions

1. Broca, P.P. Localisation des fonctions cérébrales: Siège du langage articulé. *Bull. De La Société D'Anthropologie* Tome IV 200–208 (1863).
2. Fritsch, G. & Hitzig, E. Uber die elektrische Erregbarkeit des Grosshirns. *Arch. Anat. Physiol. wissenschaftl. Med.* **37**, 300–332 (1870).
3. Felleman, D.J. & Van Essen, D.C. Distributed hierarchical processing in the primate cerebral cortex. *Cereb. Cortex* **1**, 1–47 (1991).
4. Maunsell, J.H. & Van Essen, D.C. Functional properties of neurons in middle temporal visual area of the macaque monkey. I. Selectivity for stimulus direction, speed, and orientation. *J. Neurophysiol.* **49**, 1127–1147 (1983).
5. Shipp, S. & Zeki, S. The organization of connections between areas V5 and V2 in macaque monkey visual cortex. *Eur. J. Neurosci.* **1**, 333–354 (1989).
6. Sincich, L.C. & Horton, J.C. Independent projection streams from macaque striate cortex to the second visual area and middle temporal area. *J. Neurosci.* **23**, 5684–5692 (2003).
7. Yabuta, N.H., Sawatari, A. & Callaway, E.M. Two functional channels from primary visual cortex to dorsal visual cortical areas. *Science* **292**, 297–300 (2001).
8. Movshon, J.A. & Newsome, W.T. Visual response properties of striate cortical neurons projecting to area MT in macaque monkeys. *J. Neurosci.* **16**, 7733–7741 (1996).
9. DeYoe, E.A. & Van Essen, D.C. Segregation of efferent connections and receptive field properties in visual area V2 of the macaque. *Nature* **317**, 58–61 (1985).
10. Peterhans, E. & von der Heydt, R. Functional organization of area V2 in the alert macaque. *Eur. J. Neurosci.* **5**, 509–524 (1993).
11. Hubel, D.H. & Livingstone, M.S. Segregation of form, color and stereopsis in primate area 18. *J. Neurosci.* **7**, 3378–3415 (1987).
12. Orban, G.A., Kennedy, H. & Bullier, J. Velocity sensitivity and direction selectivity of neurons in areas V1 and V2 of the monkey: influence of eccentricity. *J. Neurophysiol.* **56**, 462–480 (1986).
13. Cumming, B.G. & DeAngelis, G.C. The physiology of stereopsis. *Annu. Rev. Neurosci.* **24**, 203–238 (2001).
14. Girard, P., Salin, P.A. & Bullier, J. Response selectivity of neurons in area MT of the macaque monkey during reversible inactivation of area V1. *J. Neurophysiol.* **67**, 1437–1446 (1992).
15. Gattass, R., Gross, C.G. & Sandell, J.H. Visual topography of V2 in the macaque. *J. Comp. Neurol.* **201**, 519–539 (1981).
16. Gattass, R., Sousa, A.P. & Gross, C.G. Visuotopic organization and extent of V3 and V4 of the macaque. *J. Neurosci.* **8**, 1831–1845 (1988).
17. Prince, S.J., Cumming, B.G. & Parker, A.J. Range and mechanism of encoding of horizontal disparity in macaque V1. *J. Neurophysiol.* **87**, 209–221 (2002).
18. DeAngelis, G.C. & Uka, T. Coding of horizontal disparity and velocity by MT neurons in the alert macaque. *J. Neurophysiol.* **89**, 1094–1111 (2003).

19. Zar, J.H. *Biostatistical Analysis*, 380–382 (Prentice Hall, Upper Saddle River, New Jersey, 1999).
20. Tsao, D.Y. *et al.* Stereopsis activates V3A and caudal intraparietal areas in macaques and humans. *Neuron* **39**, 555–568 (2003).
21. Born, R.T. & Bradley, D.C. Structure and function of visual area MT. *Annu. Rev. Neurosci.* **28**, 157–189 (2005).
22. Komatsu, H. & Wurtz, R.H. Relation of cortical areas MT and MST to pursuit eye movements. I. Localization and visual properties of neurons. *J. Neurophysiol.* **60**, 580–603 (1988).
23. Newsome, W.T., Wurtz, R.H., Dursteler, M.R. & Mikami, A. Deficits in visual motion processing following ibotenic acid lesions of the middle temporal visual area of the macaque monkey. *J. Neurosci.* **5**, 825–840 (1985).
24. Dursteler, M.R. & Wurtz, R.H. Pursuit and optokinetic deficits following chemical lesions of cortical areas MT and MST. *J. Neurophysiol.* **60**, 940–965 (1988).
25. Inoue, Y., Takemura, A., Kawano, K., Kitama, T. & Miles, F.A. Dependence of short-latency ocular following and associated activity in the medial superior temporal area (MST) on ocular vergence. *Exp. Brain Res.* **121**, 135–144 (1998).
26. Busettini, C., Miles, F.A. & Krauzlis, R.J. Short-latency disparity vergence responses and their dependence on a prior saccadic eye movement. *J. Neurophysiol.* **75**, 1392–1410 (1996).
27. Takemura, A., Murata, Y., Kawano, K. & Miles, F.A. Deficits in short-latency tracking eye movements after chemical lesions in monkey cortical areas MT and MST. *J. Neurosci.* **27**, 529–541 (2007).
28. Hupé, J.M., James, A.C., Girard, P. & Bullier, J. Response modulations by static texture surround in area V1 of the macaque monkey do not depend on feedback connections from V2. *J. Neurophysiol.* **85**, 146–163 (2001).
29. Sandell, J.H. & Schiller, P.H. Effect of cooling area 18 on striate cortex cells in the squirrel monkey. *J. Neurophysiol.* **48**, 38–48 (1982).
30. Prince, S.J., Pointon, A.D., Cumming, B.G. & Parker, A.J. Quantitative analysis of the responses of V1 neurons to horizontal disparity in dynamic random-dot stereograms. *J. Neurophysiol.* **87**, 191–208 (2002).
31. Qian, N. & Andersen, R.A. A physiological model for motion-stereo integration and a unified explanation of Pulfrich-like phenomena. *Vision Res.* **37**, 1683–1698 (1997).
32. Anzai, A., Ohzawa, I. & Freeman, R.D. Joint-encoding of motion and depth by visual cortical neurons: neural basis of the Pulfrich effect. *Nat. Neurosci.* **4**, 513–518 (2001).
33. Pack, C.C., Born, R.T. & Livingstone, M.S. Two-dimensional substructure of stereo and motion interactions in macaque visual cortex. *Neuron* **37**, 525–535 (2003).
34. Bradley, D.C., Qian, N. & Andersen, R.A. Integration of motion and stereopsis in middle temporal cortical area of macaques. *Nature* **373**, 609–611 (1995).
35. Bradley, D.C., Chang, G.C. & Andersen, R.A. Encoding of three-dimensional structure-from-motion by primate area MT neurons. *Nature* **392**, 714–717 (1998).
36. Dodd, J.V., Krug, K., Cumming, B.G. & Parker, A.J. Perceptually bistable three-dimensional figures evoke high choice probabilities in cortical area MT. *J. Neurosci.* **21**, 4809–4821 (2001).
37. Grossberg, S. The complementary brain: unifying brain dynamics and modularity. *Trends Cogn. Sci.* **4**, 233–246 (2000).
38. Berzhanskaya, J., Grossberg, S. & Mingolla, E. Laminar cortical dynamics of visual form and motion interactions during coherent object motion perception. *Spat. Vis.* **20**, 337–395 (2007).
39. Pack, C.C., Conway, B.R., Born, R.T. & Livingstone, M.S. Spatiotemporal structure of nonlinear subunits in macaque visual cortex. *J. Neurosci.* **26**, 893–907 (2006).
40. Churchland, M.M., Priebe, N.J. & Lisberger, S.G. Comparison of the spatial limits on direction selectivity in visual areas MT and V1. *J. Neurophysiol.* **93**, 1235–1245 (2005).
41. Gattass, R., Gross, C.G. & Sandell, J.H. Visual topography of V2 in the macaque. *J. Comp. Neurol.* **201**, 519–539 (1981).
42. Gattass, R., Sousa, A.P. & Gross, C.G. Visuotopic organization and extent of V3 and V4 of the macaque. *J. Neurosci.* **8**, 1831–1845 (1988).
43. Albright, T.D., Desimone, R. & Gross, C.G. Columnar organization of directionally selective cells in visual area MT of the macaque. *J. Neurophysiol.* **51**, 16–31 (1984).
44. DeAngelis, G.C. & Newsome, W.T. Organization of disparity-selective neurons in macaque area MT. *J. Neurosci.* **19**, 1398–1415 (1999).
45. Chen, G., Lu, H.D. & Roe, A.W. Functional architecture of macaque cortical area V2 for depth surfaces revealed by optical imaging. *Soc. Neurosci. Abst.* 114.6 (2006).
46. Ohki, K. *et al.* Highly ordered arrangement of single neurons in orientation pinwheels. *Nature* **442**, 925–928 (2006).
47. Boyden, E.S., Zhang, F., Bamberg, E., Nagel, G. & Deisseroth, K. Millisecond-timescale, genetically targeted optical control of neural activity. *Nat. Neurosci.* **8**, 1263–1268 (2005).
48. Lomber, S.G., Payne, B.R. & Horel, J.A. The cryoloop: an adaptable reversible cooling deactivation method for behavioral or electrophysiological assessment of neural function. *J. Neurosci. Methods* **86**, 179–194 (1999).
49. Busettini, C., Masson, G.S. & Miles, F.A. A role for stereoscopic depth cues in the rapid visual stabilization of the eyes. *Nature* **380**, 342–345 (1996).
50. Takemura, A., Inoue, Y., Kawano, K., Quaia, C. & Miles, F.A. Single-unit activity in cortical area MST associated with disparity-vergence eye movements: evidence for population coding. *J. Neurophysiol.* **85**, 2245–2266 (2001).